Proc. Indian Acad. Sci. (Earth Planet. Sci.), Vol. 93, No. 3, August 1984, pp. 257–282.

Advances in microwave remote sensing of the ocean and atmosphere

P C PANDEY and T A HARIHARAN

Space Applications Centre, Indian Space Research Organisation, Ahmedabad 380053, India

Abstract. This article reviews the current state-of-the-art and future prospects of the microwave techniques for remote sensing of the earth's atmosphere and ocean. Geophysical parameters and their relationship with measured thermal microwave radiation is established through radiative transfer processes. The atmospheric temperature profile obtained from microwave sounding unit (MSU) onboard TIROS-N series of satellites is operational and is used for numerical weather prediction. The demonstrated applications of scanning multichannel microwave radiometer (SMMR) onboard most recent and advanced SEASAT satellite are highlighted: The capability of SEASAT active sensors for monitoring ocean parameters have also been indicated. Feasible applications of microwave techniques *e.g.* moisture profile with advanced moisture sounder (AMSU), and surface pressure from multifrequency active microwave pressure sounder (MPS) are also described. Finally the recent and advanced microwave limb sounding (MLS) technique and its applications to upper atmospheric research has been reviewed.

Keywords. Microwave remote sensing; geophysical parameters; thermal microwave radiation; radiative transfer; atmospheric temperature profile; SEASAT satellite; moisture profile; surface pressure; microwave limb sounding technique.

1. Introduction

During the last two decades, microwave techniques and its demonstrated applications have led to the beginning of operationalization of microwave sensors for atmospheric and oceanographic applications. Because of the cloud-penetrating capability of microwave radiation together with high stability and sensitivity of microwave radiometers, microwave measurements can significantly add to the information on atmospheric processes. Microwave techniques could also be used in active mode with their own source of illumination, but its application is restricted. In the present review, discussion is mainly devoted to the application of passive microwave radiometers.

A recent review article by Njoku (1982) summarizes recent advances in the passive microwave radiometry. Others (Tomiyasu 1974; Ulaby 1976; Swift 1980; Staelin 1981; Hariharan and Pandey 1983) have also reviewed the progress from time to time. The present article gives an overview of the current state-of-the-art in passive microwave radiometry with some important element of active sensors and recent advances in upper atmospheric research using the recent microwave limb sounding (MLS) technique. The contribution of Indian scientists to passive microwave radiometry has also been highlighted.

2. The physics of microwave radiative transfer

The concept of blackbody radiation is essential for defining the thermal radiation from geophysical sources. A blackbody is an idealized perfectly opaque material capable of

absorbing all the radiation falling on it, reflecting none. In addition to being a perfect absorber, it has also to be a perfect emitter.

According to Planck's radiation law, the brightness for a blackbody at thermal equilibrium with its surrounding is given by

$$B = \frac{2hf^3}{c^2}(1/c^{hf/kT} - 1)\,\mathrm{W/m^2/ster/Hz} \tag{1}$$

where B is the blackbody spectral brightness, h the Planck's constant, f the frequency (Hz), k the Boltzman's constant, T the absolute temperature and c the velocity of light. For microwave wavelength and at a temperature typical of the earth's atmosphere and its surface, the Rayleigh-Jeans approximation, $h\lambda/kT \ll 1$ is valid and (1) can be written in terms of wavelength ($c = f\lambda$) as,

$$B = 2kT/\lambda^2. \tag{2}$$

Earth's radiation is expressed in terms of brightness temperature, T_B. If brightness of a geophysical surface is represented by a blackbody with the same brightness, then brightness temperature of the radiation is equal to the physical temperature of the equivalent blackbody, T_B. This leads to the relationship of brightness temperature to physical temperature in terms of e, the emissivity

$$T_B = eT, \tag{3}$$

where e, which is a function of the physical form and the composition of the material and is less than 1 for radiating bodies encountered in nature.

The radiometers, however, provide antenna temperatures, defined through the following integral equation

$$T_A = \frac{1}{4\pi}\int_\Omega T_B(\Omega)G(\Omega)\,\mathrm{d}\Omega, \tag{4}$$

where $G(\Omega)$ is antenna gain. The brightness temperature is however the desired quantity. Therefore, one should generally choose a narrow-beam antenna with very low sidelobes to avoid the problems associated with inverting integral equations. Detailed inversion methods are described by Njoku (1980) and applied for SEASAT-SMMR data.

For a downward looking spaceborne radiometer over the oceans, the components of radiative transfer equation are given by

$$T_B = T_1 + T_2 + T_3 + T_4, \tag{5}$$

where

$T_1 (= \varepsilon T_s e^{-\tau_0})$ is the surface radiance, attenuated by atmosphere,

T_s the surface temperature,

$\tau_0 \left(= \int_0^\infty \alpha(u)\,\mathrm{d}u\right)$ the total atmospheric opacity,

T_2 the upwelling atmospheric radiation

$$= \int_0^\infty T(h)\alpha(h)\exp\left[-\int_h^\infty \alpha(u)\,\mathrm{d}u\right]$$

$T(h)$ = atmospheric temperature profile,

T_3 = downwelling atmospheric radiance, reflected by the surface and attenuated by the intervening atmosphere

$$= r \int_0^{\infty} T(h)\alpha(h) \exp\left[-\int_0^{h} \alpha(u)\, du \right] \cdot e^{-\tau_0},$$

$r(=1-\varepsilon)$ the reflectivity,

ε = surface emissivity,

T_4 = cosmic background temperature, downward attenuation, reflection from the surface and again attenuation in upward propagation,

$\alpha(h)$ = total absorption due to oxygen, water vapour and cloud at height h.

Figure 1 shows the various components of the radiative transfer equation. Thus brightness temperature measured by a radiometer potentially contains information about atmosphere and the surface parameters which could be retrieved using multifrequency measurements.

The emissivity of a calm sea surface is calculated from Fresnel formula and is a function of look angle and complex dielectric constants which in turn is a function of Debye parameters—the static dielectric constants, the relaxation time and the ionic conductivity. The Debye parameters have been tabulated as a function of temperature and salinity by Saxton and Lane (1952). The emissivity of a wind-driven and foam-covered sea is obtained from the emissivity models developed by Wilheit (1979) and by Pandey and Kakar (1982). Pandey and Kakar (1982) have used the SEASAT-SMMR data and the empirical wind speed dependence by Hollinger (1971) in their emissivity model and is valid for frequencies below 40 GHz.

The earth's atmosphere affects the brightness temperature through the opacity term which depends upon the absorption due to various atmospheric constituents. The principal absorbing constituents of electromagnetic radiation in the microwave region are H_2O, O_2, hydrometeors and many trace gases including $O_3, CO, H_2O_2, ClO, O, OH$,

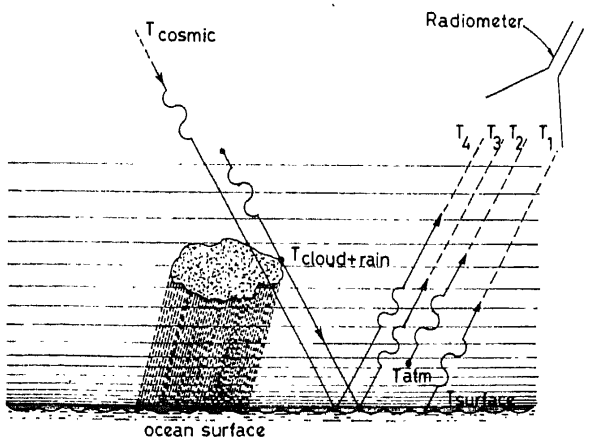

Figure 1. Radiative transfer components of a downward looking radiometer.

and various oxides of nitrogen. An excellent treatment of the absorption due to various atmospheric gases and trace constituents is given by Waters (1976). The various absorption formalisms are accurate enough for general remote sensing applications but there is still some debate on the role of water vapour dimers and its effect on remote sensing which may be important if relative humidity is high. This and some other issues like line shape and in some cases line strengths require further research.

3. Basic principles of microwave radiometers

Figure 2 is a block diagram of the Dicke-microwave radiometer system, which consists basically of a high gain antenna, a Dicke switch, a noise source, predetection section, square law detector, synchronous demodulator and integrator. The predetection section consists of the RF amplifier, mixer and IF amplifier characterized by a predetection power gain G and bandwidth B. The Dicke switch provides modulation by switching the receiver input between the antenna and a reference noise source at a rate higher than the highest significant spectral component in the gain variation spectrum. Both the switch and synch detector are driven by a square-wave generator so that the radiometer alternately views the incoming radiation and a stable reference load maintained at a constant temperature. As a result of coherent detection, the d.c. integrated output is given by

$$V = ckBG(T_0 - T_A), \tag{6}$$

which is independent of the receiver noise T_{RN}, a problem encountered in the total power radiometer system. In (6), T_A is the antenna temperature and T_0 is the constant temperature of the reference load.

Either a dish type or phased arrays antenna has normally been used in passive microwave radiometry. Parabolic dish with a feed or collecting horn at the focus has been used. In multifrequency observations a single collecting horn or feed receives all the wavelengths coaxially. A further variation is the offset parabolic dish with a feed placed off the main axis. An example is the SEASAT-SMMR antenna system. This has the advantage of not shadowing the dish—an important factor where high sensitivity is required.

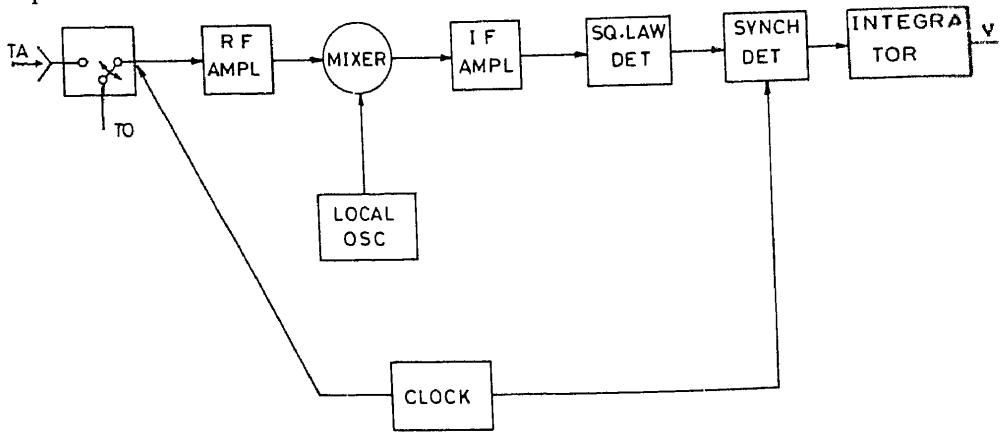

Figure 2. Block diagram of a Dicke microwave radiometer.

A phased array consists of rectangular array of waveguide sections feeding slot-shaped antenna elements. Phase shifters are employed to give electronic scanning of the antenna beam.

The sensitivity of the radiometer is given by

$$\Delta T_B = K(T_A + T_s)/\sqrt{B\tau}, \tag{7}$$

where K is a constant and varies with radiometer type and T_s is the system noise temperature. For most mission todate, the instruments have sufficient bandwidth and integration time (τ) to achieve a 0·3–0·5 K resolution over a wide scan angle.

Spatial resolution is another quantity of interest in microwave radiometry and is dictated by antenna beamwidth.

$$d = \lambda H/D, \tag{8}$$

where d is the diameter of the resolution cell (the footprint), H is the satellite altitude and λ/D is the antenna beamwidth, where λ is the electromagnetic wavelength and D is the diameter of the antenna aperture. For more details of different types of radiometers, see Ulaby *et al* (1981).

4. Microwave sensors used in R and D and operational satellites

Table 1 shows the evolution of passive microwave radiometers along with instrument capability and characteristics. The first satellite-based microwave observations of earth were made with Kosmos-243 (Basharinov *et al* 1969). The U S *Nimbus* series of the satellites have given most extensive measurements, with accelerated activity in 1978, when SEASAT and *Nimbus-G* were launched. The success of the various instruments, active and passive onboard SEASAT and the scientific results obtained from them have added a new dimension to our capability for monitoring the ocean from space. The recent MLS technique for monitoring and observing upper atmospheric parameters is another example of the unique capability of microwave technique (Waters and Wofsky 1978).

SEASAT was possibly the only satellite launched by NASA to demonstrate the usefulness of the active and passive microwave sensors for oceanographic applications. It was a proof-of-the concept mission and its success has triggered an international interest in monitoring oceans from space using microwave sensors. Table 2 lists the different sensors onboard SEASAT with the principal geophysical parameters retrieved from each sensor. The method of sensing is also mentioned. Table 3 gives the swath of the instruments except synthetic aperture radar whose processing is entirely different from the other active sensors.

The SMMR, also placed on *Nimbus-G*, is possibly the best among the recent microwave radiometers flown from the satellite platform. The instrument measured microwave radiation at 6·6, 10·69, 18, 21 and 37 GHz both in horizontal and vertical polarizations, giving ten measurements. The antenna system comprises a 42° offset parabolic reflector illuminated by a single feedhorn covering the entire range of wavelengths and providing coaxial antenna beams for all channels. Scanning is achieved by oscillating the reflector sinusoidally about a vertical axis through the feed horn resulting in a conical scan pattern with the angle of incidence constant on the surface of the earth near 50°. The scan is aft looking and is biased towards the right of the flight path so that the centre of the swath is 22° from the orbital track. Details of SEASAT SMMR instrument charac-

Table 1. History of microwave radiometry on spacecraft (after Staelin 1981; Njoku 1982 with additions).

Year of Launch	Spacecraft/ instrument acronym	Frequencies (GHz)	Antenna type	Smallest resolution element (km)	Principal parameters measured or inferred
1962	Mariner 2 (Venus flyby)	15·8, 22·2	Mechanically scanned parabola	13000	Limb darkening of planetary emission
1968	Cosmos 243	3·5, 8·8 22·2, 37	Nadir-viewing horns	13	Atmosphere: water-vapour content, liquid-water content Surface: Sea temperature, sea-ice concentration.
1970	Cosmos 384	—	—	—	
1972	Nimbus 5 ESMR	19·3	Electrically scanned array	25	Atmosphere: Rain rate Surface; Sea-ice concentration, ice classification, snow cover.
	NEMS	22·2, 31·4 53·6, 54·9 58·8	Five lens loaded horns, nadir-viewing	200	Atmosphere: Temperature profile, water-vapour content, liquid water content. Surface: Ice classification, snow cover
1973	Skylab S193	13·9	Mechanically scanned parabola	16	Surface: Soil moisture, ocean winds Atmosphere: Rain rate
	S194	1·4	Nadir-viewing phased array	115	Surface: Soil moisture.
1974	Meteor	37	Dual polarisation 30° from nadir	—	Atmosphere: Liquid water content
1975	*Nimbus* 6 ESMR	37	Dual polarisation electrically scanned array	20 × 43	Same as *Nimbus* 5 ESMR
	SCAMS	22·2, 31·6 52·8, 53·8, 55·4	Three rotating hyperbolic mirrors	150	Same as *Nimbus* 5 NEMS

1978	DMSP SSM/T	50·5, 53·2, 54·3, 54·9, 58·4, 58·8, 59·4	Single rotating mirror	175	Atmosphere: Temperature profile
1978	TIROS-N/MSU (2 satellites)	50·3, 53·7, 55, 57·9	Dual rotating mirrors	110	Atmosphere: Temperature profile
1978	*Nimbus*-7 SMMR	6·6, 10·7, 18, 21, 37	Single oscillating offset parabolic reflector	18 × 27	Atmosphere: Water vapour content, liquid water content, rain rate
	SEASAT 1 SMMR	-do-	—	14 × 21	Surface: Sea state (wind speed) sea temperature, sea-ice concentration, ice classification, snow cover, soil moisture
1979	*Bhaskara*-I SAMIR	19·4, 22·2	Lens corrected horns	150 230	Atmosphere: water vapour content, liquid water content.
1981	*Bhaskara*-II SAMIR	19·4, 22·2, 31·4	Lens corrected horns	150	Atmosphere: water vapour content, liquid water content Surface: ocean winds
1983 (planned)	DMSP SSM/I	19·1, 22·3, 37, 85·5	Continuously rotating offset parabolic reflector	16 × 14	Precipitation rate over ocean/land, ocean wind speed, ice type/concentrations, soil moisture
1986 (planned)	TIROS-0 AMSU	18·5, 22·2, 31·6, 50·3–57·9 (7 ch), 90, 150, 183·3 (3 ch)	Continuously scanned mirrors	15	Atmospheric temperature and water vapour profiles

Table 2. SEASAT remote sensing instruments.

Instrument	Type	Geophysical Measurement	Sensing Method
Altimeter (ALT)	Active short pulse radar. 13·5 GHz	Wave height altitude above near sea level surface and wind speed at Nadir.	Return pulse-wave from delay time to mid point and backscatter coefficient.
Microwave scatterometer	Active 14·6 GHz	Surface wind speed and direction.	Radar backscatter–increases with wind speed; forward and AFT beam data determine direction.
Synthetic aperture radar (SAR)	Active imaging 1·275 GHz	Wave spectra	Radar echo-range or time delay and frequency shift: forms brightness image.
Scanning multichannel microwave radiometer (SMMR)	Passive 6·6, 10·69, 18·0, 21·0, 37 GHz both horizontal and vertical polarization	Surface wind speed, sea surface, temperature atmospheric water content.	Receives and measures several microwave frequencies, each one sensitive to a particular geophysical parameter.
Visible and Infrared radiometer	Passive imaging 0·49 to 0·94 μm visible 10·5 to 12·5 μm IR	Sea surface and cloud top mean temperature; ocean coastal and atmospheric feature location.	Receives and measures visible and IR emissions.

Table 3. Sensor coverage.

	Sensor			
Swath	ALT	SASS	SMMR	VIRR
Width (km)	2·4–12 depending on sea state	(i) Two 500–750 swaths (400 km apart) (ii) One central swath 140 km	595	2250
Position	Centered on Nadir	(i) At either side of Nadir (ii) Centered on Nadir	To the right of Nadir	Centered on Nadir

Table 4. Grid cell and footprint dimension.

	Swath width, 595 km			
Frequency (GHz)	Grid dimension	No. of cells in swath	Cell dimension (km)	Footprint dimensions (km)
6·6	1	4	149 × 149	136 × 89
10·69	2	7	85 × 85	87 × 87
18	3	11	54 × 54	54 × 35
21	3	11	54 × 54	44 × 29
37	4	22	27 × 27	28 × 18

teristics are described by Njoku (1980) and that of *Nimbus-G* SMMR by Gloersen and Barath (1977). The resolution cell of each SMMR channels is given in table 4. A special JGR issue describes the results from SEASAT (Bernstein 1982).

4.1 *Indian effort in microwave remote sensing; satellite microwave radiometer* (SAMIR) *on board Bhaskara I and II satellites*

The history of the microwave radiometry programme in India is new. A beginning in passive microwave radiometry was made with the launch of the *Bhaskara-I* satellite on 7 June 1979, an experimental satellite for earth observation with a two-channel (19·35 and 22·235 GHz) satellite microwave radiometer on board (SAMIR-I). Data from these radiometers provided the first major opportunity to Indian scientists to experience and learn different analysis techniques. The instrument details and the first scientific results were reported by Pandey *et al* (1981). A special technical report was brought out by ISRO highlighting the significant achievement of the Indian scientists (Pandey *et al* 1981) in analyzing and understanding the *Bhaskara* data. Having recognised the benefits from SAMIR-I India launched *Bhaskara-II* (SAMIR II) on 20 Nov. 1981, another experimental earth observation satellite with a three-channel (19·35, 22·235 and 31·4 GHz) radiometer. The primary purpose of SAMIR I and II was to provide data on precipitable water over Indian ocean regions which could be used along with other satellite data

from different sources for a study of the onset of the Indian monsoon and the formation of the tropical cyclones.

Both the *Bhaskara* spacecrafts were designed to operate the SAMIR system, a Dicke-type superheterodyne receiver, in two modes. In normal mode, the spin axis of the spacecraft was maintained perpendicular to the orbital plane and consequently during each spin the SAMIR observation was taken along the satellite ground trace in different view angles with respect to nadir direction. In normal mode the view angles were $\pm 2{\cdot}8°$, $\pm 5{\cdot}6°$ for 19·35 GHz and $\pm 2{\cdot}8°$, $\pm 11{\cdot}2°$ for 22·235 GHz radiometer for SAMIR-I radiometer. For SAMIR-II, the view angles for all the three channels were $\pm 2{\cdot}8°$ and $\pm 5{\cdot}6°$. Both SAMIR I and II observed zenith temperatures also. In alternate mode the spin axis of the satellite was aligned tangentially to the orbital plane at certain latitudes and consequently SAMIR radiometers could scan across the satellite ground trace at a number of angular positions ($\pm 2{\cdot}8°$, $\pm 8{\cdot}4°$, $\pm 14{\cdot}0°$, $\pm 19{\cdot}6°$, $\pm 25{\cdot}2°$, $\pm 30{\cdot}8°$, $\pm 36{\cdot}4°$). The spin rate of the spacecraft was controlled between 6 and 8 rpm for both these modes.

A long-term statistical analysis of the sensitivity of the radiometers gave $\Delta T \sim 1$ to 2K which was within the design goal of the radiometers.

5. Data processing and geophysical algorithms

The antenna temperature measured by a microwave radiometer is telemetered as signal counts from the satellite and is received on ground by earth station. The following preprocessing is done on digital counts, before geophysical parameters are extracted. (i) instrument calibration, (ii) standard cell generation, (iii) sidelobe pattern correction, (iv) polarization cross-coupling correction and (v) Faraday rotation correction. The above preprocessing sequence was followed for SEASAT SMMR and is true in principle for other radiometers also. Choice of the levels of preprocessing is decided on the accuracy requirements of the geophysical parameters and the complexity involved in their implementation.

Instrument calibration is based on prelaunch thermal-vacuum chamber and laboratory tests and is updated after launch during a validation period. Temperature-dependent losses are also monitored and telemetered along with signal counts. The antenna temperature is determined as a function of signal counts and system component temperatures. For ease of interpretation the data are averaged onto square cells (table 4) and the channels with the equal cell dimensions are used for parameter retrieval.

The antenna receives the radiation mainly through its main beam but substantial radiation enters through its sidelobe and a correction has to be applied so that the corrected value represents the true brightness temperature of the mainbeam footprint area only. The problem becomes severe near coastal regions when the energy is received from the land with high emissivity through sidelobes. The sidelobe contributions are removed using laboratory measured antenna radiation pattern and by a procedure described by Njoku *et al* (1980). The fact that horizontal polarization receiver also receives vertical polarization should be considered.

The presence of electrons and geomagnetic fields in the ionosphere causes Faraday rotation of the electromagnetic radiation. Knowing the models of the controlling factors, a correction can be applied to the data. The correction is inversely proportional

to frequency and thus the correction for high frequency channel may not be needed at all.

In Bhaskara SAMIR, the raw counts (0–127) were converted to brightness temperature using prelaunch calibration curves obtained from thermovac chamber data in the laboratory. Besides, earth location in terms of latitude and longitude of each *Bhaskara* cell was also generated by the Data Product Group of Space Applications Centre, Ahmedabad. However, no attempt was made to decouple the polarization mixing and subsequent water vapour retrieval using alternate mode data. An attempt is underway to develop statistical algorithm for polarisation decoupling and analysis of alternate mode data.

5.1 *Retrieval method*

Once the series of corrections have been applied, the result is a fully calibrated brightness temperature at all the measurement frequencies. There are two basically different methods of extracting geophysical parameters from multiwavelength measurements. The first is by statistical inversion (Waters *et al* 1975; Grody 1976; Wilheit and Chang 1980; Hofer and Njoku 1981; Pandey and Kakar 1983), the second by nonlinear iterative solution (Wentz 1982; Chahine 1977). Fourier transform technique (Rozenkranz 1978) and Kalman-Bucy filtering technique (Ledsham and Staelin 1978) have also been described in the literature and applied in certain specific cases. The most generally used procedure is statistical inversion, first used by Waters (1975) for retrieving temperature profile from measurements near 60 GHz O_2 line. The principle behind this method is to find the linear predictor D

$$\mathbf{p} = D \cdot \mathbf{T}_B \tag{9}$$

by minimizing $E\{(\mathbf{p}-\hat{\mathbf{p}})^T(\mathbf{p}-\hat{\mathbf{p}})\}$. This is of course a classical problem of multiple linear regression with elements of D given by

$$D = E\{p \cdot T_B^T\} E\{T_B T_B^T\}^{-1}. \tag{10}$$

Both the expectation values in the above expressions are covariance matrices. Instead of evaluating D as given in (10), sometimes it is more convenient to subtract mean of parameter $\mathbf{p}$ and brightness temperature $\mathbf{T}_B$. If we have large samples of measured T_B with our radiometer and also have independent direct measurements from radiosonde, ships or rocketsonde, then we can estimate D entirely from the experiment. Otherwise radiative transfer modelling with known physics and the *a priori* statistics is used to estimate D.

Nonlinear iterative technique (Chahine 1977) can also be used for retrieving moisture profile. The basic principle is that a guess is first made for the values of the geophysical parameters and the environmental model is then used to calculate the resulting brightness temperatures for each radiometer channel. These are compared with the measured brightness temperatures and residuals found. Differential correction is then applied, yielding an updated value of each geophysical parameter which in turn is applied to the environmental model. This iterative process is carried out until the difference between the calculated and measured are minimum. This method, in principle, should give better results than statistical inversion since no attempt is made to linearise the expression of brightness temperature in terms of geophysical parameters.

6. Geophysical applications

6.1 *Temperature profile*

Waters *et al* (1975) reported the first retrieval of temperature profile from NEMS onboard *Nimbus*-5 satellite using 53·65, 54·9 and 58·8 GHz brightness temperature measurement from MSU. The measurement near 60 GHz oxygen channel is proportional to atmospheric temperature at altitude defined by their weighting function, since the mixing ratio of the oxygen in the atmosphere is quite uniform and time invariant. An rms accuracy of $\sim 2°K$ has been reported by Waters (1975).

Staelin *et al* (1975) studied the effect of clouds on temperature profile retrieval and concluded that less than 0·5% sounding, mostly in the region of inter tropical convergence zone (ITCZ) is affected by clouds. Figure 3 shows the example of warm core study of a cyclone by MSU data.

In addition to ~ 60 GHz O_2 line, 118 GHz resonance line of O_2 holds a great promise for atmospheric temperature sounding. In figure 4, a set of weighting functions near 118 GHz are shown.

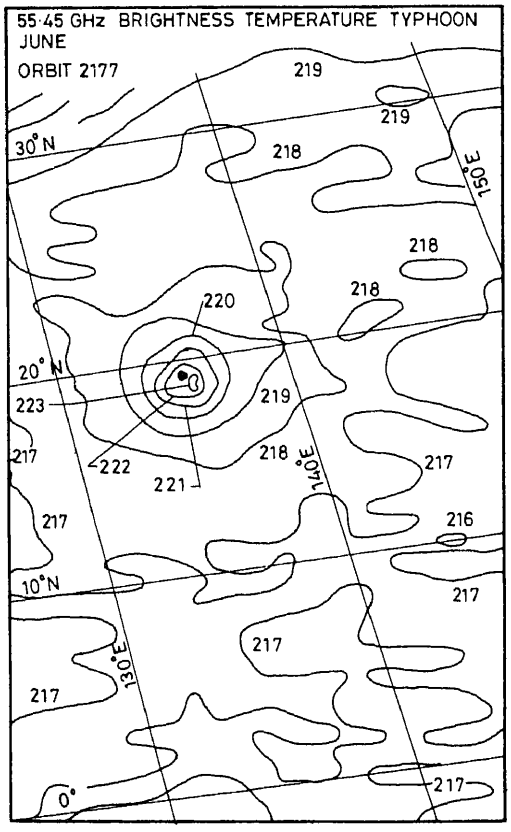

Figure 3. 55·45 GHz brightness temperature, corrected for scan angle from typhoon June on 21 November 1975. The black dot represents the eye location reported by reconnaissance aircraft (Rosenkranz *et al* 1978).

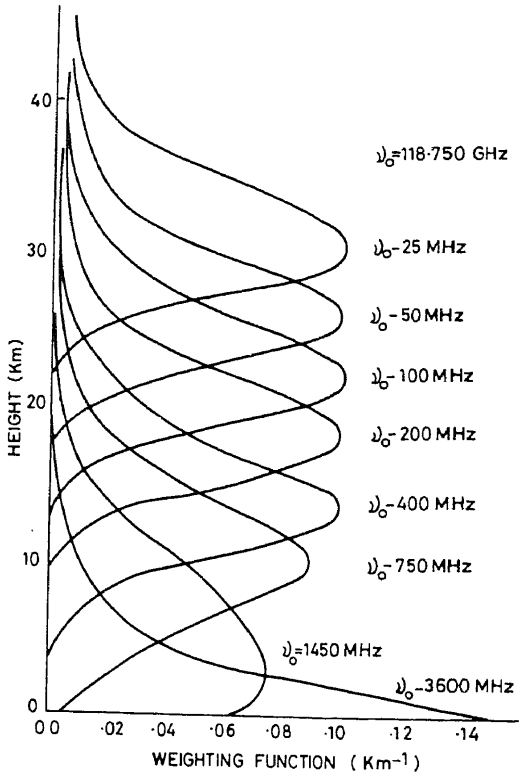

Figure 4. Temperature weighting functions near the 118 GHz oxygen line.

6.2 *Moisture profile*

Development of the radiometers (advanced moisture sounder, AMSU) employing 183 GHz water vapour line and more transparent 22 GHz line would provide moisture profile for numerical weather prediction. Research work in this direction is progressing in USA, both in terms of instrument development as well as profile retrieval technique (Schaerer and Wilheit 1979; Rosenkranz and Staelin 1982). Although no spacecraft and aircraft instrument have demonstrated this technique, theoretical simulations show an accuracy of $\sim 20\%$ per 2–3 km layer assuming known temperature profile to an accuracy of $\sim 1{\cdot}5$ K. Careful study and actual experiment are required for more definitive results. Haydu and Krishnamurthy (1981) have demonstrated the use of radiosonde data and total satellite derived water vapour content for water vapour profile retrieval making certain simplifying assumptions.

6.3 *Precipitable water and liquid water content*

The 22 GHz water vapour line has extensively been used both in NEMS and SCAMS on *Nimbus*-5 and *Nimbus*-6 satellites for water vapour and liquid water content retrieval (Staelin *et al* 1976; Grody 1976). An rms accuracy of $\sim 0{\cdot}4$ g/cm^2 for water vapour and

theoretical rms accuracy ~ 0·01 g/cm^2 for cloud liquid was obtained, since there was no experimental comparison for cloud liquid water.

Global maps of precipitable water and cloud liquid contents have also been generated using SMMR data on *Nimbus* and SEASAT satellites (Pandey 1982; Njoku and Swanson 1983; Prabhakara *et al* 1982). An example of the global distribution of precipitable water is given in figure 5. Major climatological features are revealed in the map and are possibly connected with large scale circulation features. For example, the high moisture content of the summer monsoon over the northern Bay of Bengal and the Arabian sea may be noted. Figure 6 shows another example of global distribution of liquid water content and water vapour content over Pacific ocean obtained from NEMS measurements. However, SEASAT-SMMR provided measurements at a much finer scale than the earlier NEMS and SCAMS, (Alishouse 1982).

Grody (1976) and Gohil *et al* (1982) have also studied the variation of water vapour and liquid water in cyclones and figure 7(a) is shown as an example obtained from the Indian satellite *Bhaskara*-I (Pandey *et al* 1981; Hariharan and Pandey 1983; Pathak *et al* 1983; Desai 1982). Figure 7(b) shows an example of moisture distribution from SAMIR-II onboard the third Indian satellite *Bhaskara*-II from 25 May to 25 June 1982. The instrument description, its performance and the retrieval technique has been described by Pandey *et al* (1983). All these retrievals are accurate over the oceanic regions only which provides a relatively cool and uniform background against the atmospheric emission.

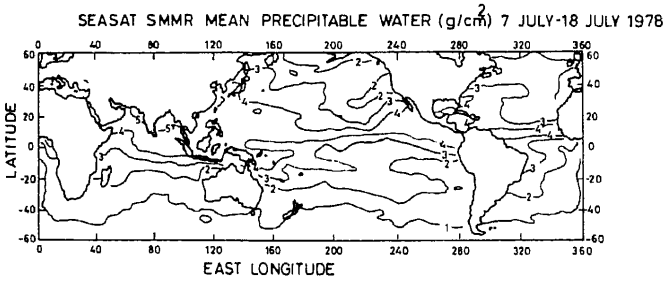

Figure 5. Global SEASAT-SMMR mean monthly moisture field for the period 7 July–18 July 1978 (Pandey 1982).

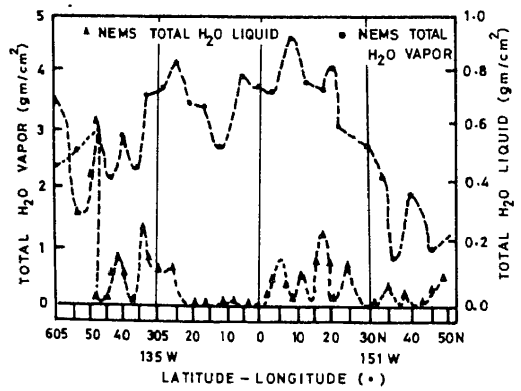

Figure 6. Global distribution of liquid water content and water vapour content over Pacific ocean obtained from NEMS (Grody 1976).

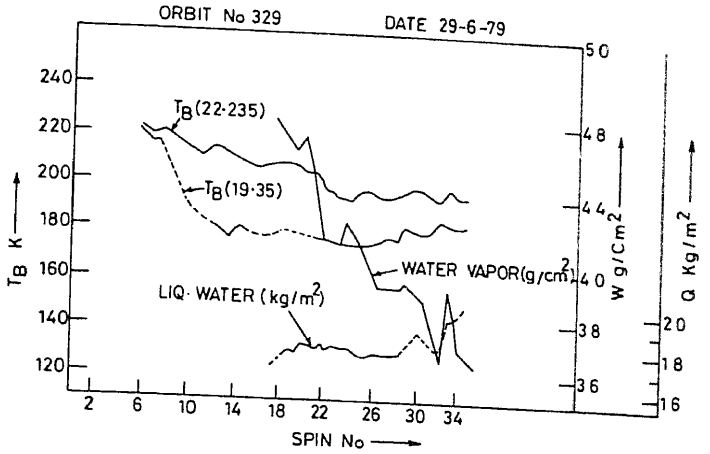

Figure 7(a). Variation of water vapour and liquid water contents in a tropical depression on 29 June 1979 obtained from SAMIR onboard the Indian Satellite *Bhaskara*-I (Gohil *et al* 1981).

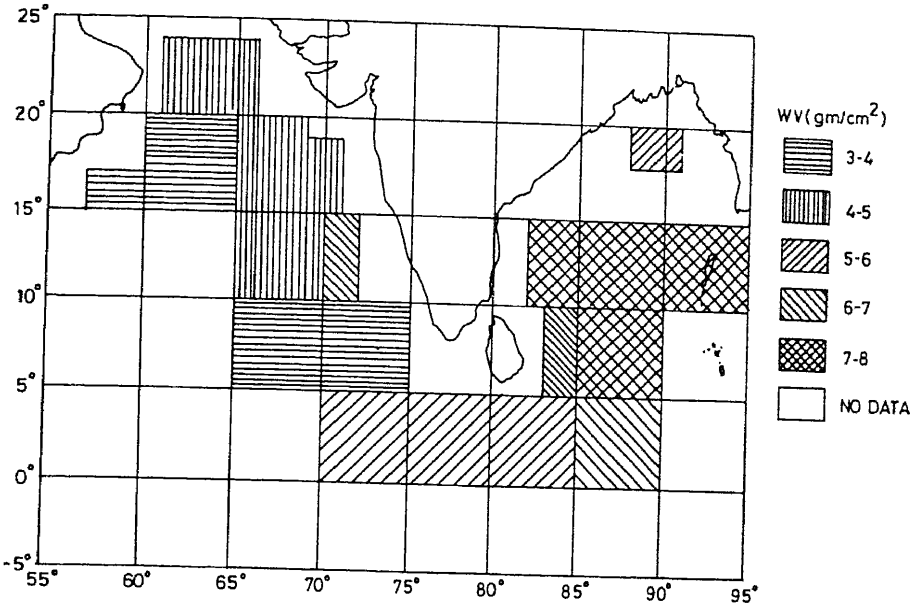

Figure 7(b). Distribution of average precipitable water derived from *Bhaskara*-II SAMIR-II, over oceans adjoining India for the period 25 May to 25 June 1982 (Pandey *et al* 1983).

6.4 *Precipitation*

Rainfall rate is an important and difficult parameter to be measured from space. A model for quantitatively relating microwave brightness temperature to rain rate over oceanic region was first developed by Wilheit *et al* (1977). Figure 8 shows the relation between Tb *vs* rainfall rate. The solid line in the figure is the calculated brightness temperature for a 4 km freezing level. The dashed curve shows the departure from the

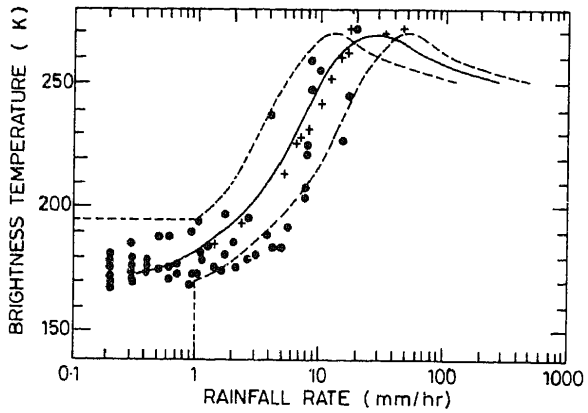

Figure 8. Brightness temperature as a function of rain rate: (•) *Nimbus*-5 ESMR *vs* WSR-57 radar; (+) inferred from ground-based measurements of brightness temperature and direct measurement of rain rate (Wilheit *et al* 1977).

calculated brightness temperature. Wilheit *et al* (1977) quoted an error of $\sim 100\%$ in rainfall rate estimation.

Rainfall rate in tropical cyclones has also been reported (Allison *et al* 1974). Adler and Rodgers (1977) used *Nimbus*-5 ESMR data to calculate the latent heat release in a tropical cyclone. They concluded that these observations were potentially useful in monitoring tropical cyclones for observing the change from a weak system to a strong system.

A workshop report (Atlas and Thiele 1982) points out strongly the importance of precipitation measurements from space and a number of recommendations using both active and passive technique (hybrid) and both IR and microwave (MW) sensors.

Another useful development for precipitation measurements from space is the utilization of ~ 90 GHz channel, currently on defence meteorological satellites programme (DMSP). The initial studies and recommendation for 90 GHz channel were made by Savage (1976). More theoretical and experimental work in this direction has been initiated (Weiman and Davies 1978; Wilheit *et al* 1982).

6.5 *Sea surface temperature*

SMMR onboard SEASAT and *Nimbus* is the first and most recent satellite-borne microwave radiometer to provide global measurement of sea surface temperature. Comparison with high quality *in situ* observations of SST indicated an rms accuracy of $\sim 1{\cdot}5$ K in SST retrieval (Hofer *et al* 1981; Pandey and Kakar 1983; Lipes 1980). Global maps of SST and its comparison with climatological map are shown in figure 9. An attempt is made to ensure the reliable reproduction of SST anomalies which could be used for weather forecasting and climatic studies. SMMR-SST contour maps compares favourably with the climatological map. However, the contour near coastal regions and inland waters may be considered with suspicion but in areas 600 km away from main island, the contours are believed to be reliable to within 1–1·5 K. Further advances have also been made to evaluate the effectiveness of one to three channel radiometers in retrieving SST (Pandey and Kniffen 1982). The results indicate the promise of three-channel subset for SST

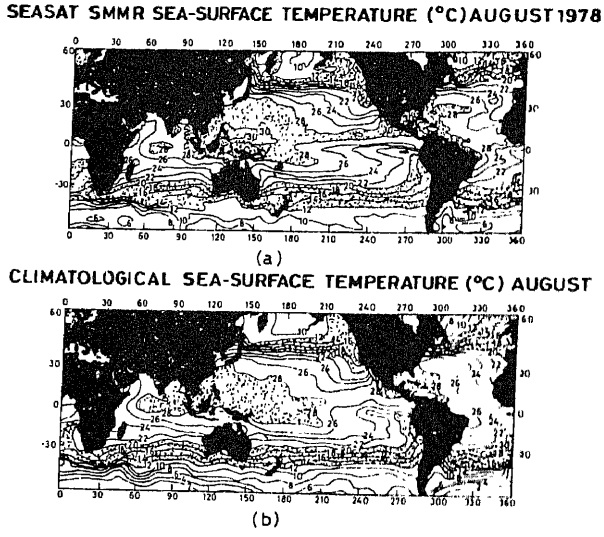

Figure 9a. SEASAT SMMR SST, **b.** Climatological SST map, for August 1978 (Njoku and Swanson 1983).

retrieval but more comparisons and evaluations are needed under different weather conditions before one can conclude the ultimate capability of these subsets, which may reduce the cost of instrumentation in future generation of satellites. Earlier, Blume *et al* (1978) measured SST using 2·65 GHz radiometer from an aircraft and concluded that an accuracy ~ 1 K is feasible.

NASA, because of importance of SST for oceanic processes and studies relating to weather and climate, planned a series of workshops at the Jet Propulsion Laboratory in 1983 to evaluate both IR and MW sensors for SST retrieval. An rms accuracy of 0·5 2K has been reported with the existing IR and MW sensors. Future workshops will recommend the configuration of the future sensor to be flown on the next generation of satellites

6.6 *Ocean surface wind*

SEASAT-SMMR provided global measurement of wind speed (Bernstein 1982). Point comparison with *in situ* observations showed an rms accuracy of 2·5 m/sec over different oceanic regions of the world (Pandey 1983; Lipes 1980; Njoku 1983). Figure 10 shows the global mean map of windspeed for the entire SEASAT mission life (7 July 10 October 1978). Mean monthly global maps of windspeed have also been generated from SMMR and compared with altimeter and scatterometer windspeed (Pandey 1983). There was an overall agreement between windspeed obtained from the three sensors, with biases noted in certain latitude belts, requiring further studies.

6.7 *Salinity*

Aircraft studies have been reported with microwave sensors for measuring salinity over oceans (Thomann 1976; Blume *et al* 1978). Blume *et al* (1978) used nadir looking *S* and *L* band radiometers to map both surface temperature and salinity synoptically. The

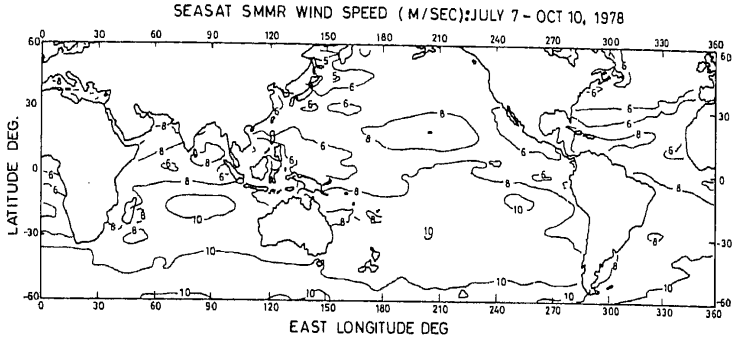

Figure 10. Global distribution of SEASAT-SMMR windspeed for the period 7 July–10 Oct 1978 (Pandey 1983).

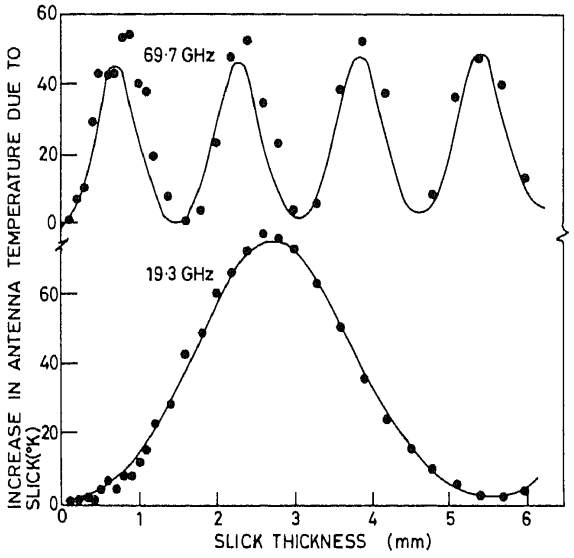

Figure 11. Increased brightness temperature *vs* oil slick thickness at 69·75 and 19·34 GHz (Hollinger 1974).

results were compared with the chemical analysis of the sample and the rms deviations were found to be less than 1 ppt.

6.8 *Oil spills*

Hollinger and Mennella (1973) and Hollinger (1974) conducted laboratory and field measurement of oil slick thickness. The results of their laboratory measurements are shown in figure 11. Based on the feasibility of laboratory experiment, a cooperative programme was initiated between the Naval Research Laboratory (NRL), the Virginia Institute of Marine Sciences NASA/Wallops, USA and the US Coast Guard to observe the time development of a controlled oil spill spread. The field result demonstrated that microwave radiometers can be used to measure slick thickness of less than a mm.

6.9 *Snow and ice*

Electronically scanning microwave radiometer (ESMR) onboard *Nimbus*-5 provided the first synoptic view of the Arctic and Antarctic sea ice and ice sheets (Campbell *et al* 1980). The time lapse motion picture film made from ESMR images showed many interesting results not noticed earlier (Gloerson *et al* 1978). Wilheit *et al* (1972) showed the possibility of distinguishing sea ice from liquid water both through the clouds and in the dark, which was important to observe leads and polynyas. Kunzi *et al* (1976) also used the NEMS data for distinguishing different types of snow and ice. SMMR on *Nimbus*-7 is currently being used extensively for sea ice studies, iceberg, ice, difference between first year and multiyear ice etc., and snow studies.

6.10 *Soil moisture*

The success of passive microwave radiometry is more for measuring ocean parameters than for land-based applications. Studies using both active and passive sensors (Ulaby 1975; Moore and Young 1977; Schmugge *et al* 1974; Schmugge 1978) have been reported for soil moisture studies. Schmugge *et al* (1974) suggested frequencies near 1·4 GHz for soil moisture determination, which for a satellite platform would require, a large antenna for getting ground resolutions suitable for most of the applications. Various ground-based experiments are also in progress (Newton 1976). The presence of soil moisture causes a marked change in soil dielectric properties, resulting in a decrease in emissivity over that of a dry soil. In addition to the presence of moisture, surface roughness and vegetation cover also have significant effects, generally tending to increase the surface emissivity. Figure 12 shows the results of an aircraft flight over a vegetated field as reported by Schmugge (1976).

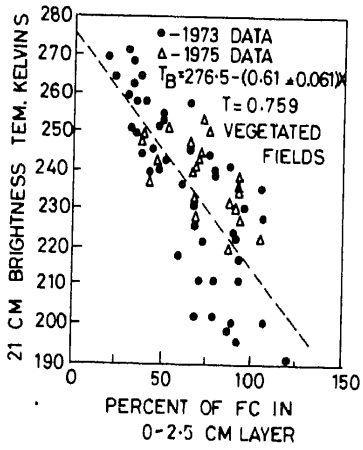

Figure 12. Aircraft observations of TB over vegetated agricultural fields around Phoenix, Arizona for the years 1973 and 1976 (Schmugge 1976).

6.11 *Surface pressure*

The MPS programme is currently under development at Jet Propulsion Laboratory, USA. The other organizations involved are Heriot-Watt University, Edinburg and the Rutherford Appleton Laboratory, UK (Flower 1978). Theoretical investigations have been carried out to optimize the sensor parameters for measuring surface pressure (Pekham and Flower 1983; Gately *et al* 1983). Feasibility of retrieving ocean surface wind, precipitable water and cloud liquid water has also been investigated using MPS, an active sensor. The method is based on the principle of making active multifrequency measurements near 60 GHz oxygen line and determining the ratios of the atmospheric transmissivities. The ratio of transmissivities or differential absorption is a measure of the total oxygen in the path and hence on the partial pressure of the oxygen at the surface. Since oxygen is a uniformally mixed constituent of dry air, this is also a measure of the total surface pressure. Differential absorption measurements at the other two pairs of frequencies are necessary to make the measurement insensitive to atmospheric temperature profile, water vapour content, cloud cover and sea state. The tentative frequencies selected are 29·2555, 36·5555, 44·80, 52·80, 67·51 and 73·01 GHz (Flower *et al* 1978). Theoretical simulations have shown the capability of measuring surface pressure to an rms accuracy of 2mbar. Recent experimental flight of MPS at JPL has shown very encouraging results for surface pressure measurements.

6.12 *Cloud temperature and geometrical thickness*

Numerical simulations have been performed by Pandey *et al* (1983), for the first time, to determine the feasibility of retrieving cloud temperature and its geometrical thickness from multifrequency (SMMR) and concurrent IR measurements. Recently, it has been demonstrated that cloud top height and fractional coverage can be estimated from IR measurements, under a variety of atmospheric conditions. However, it appears that cloud temperature and its geometric thickness cannot be determined using IR, because of the opacity of clouds in IR. The simulation result using IR and MW technique indicated the possibility with an rms error of $\sim 0{\cdot}4$ km in thickness and about $\sim 3°C$ in cloud temperature retrieval.

7. Passive microwave radiometry for upper atmospheric applications

A very active and advanced research programme for microwave sensing of upper atmosphere using high resolution microwave radiometric technique (limb sounding technique) is being pursued by Waters (1978) and his colleagues at Jet Propulsion Laboratory, USA. The application review panel set up by NASA (Staelin and Rosenkranz 1978) has given a very high priority to the development of limb sounding technique, which has the potential of providing information of stratosphere, mesosphere and thermosphere, not provided by any other technique. The limb sounding technique, its potential, future prospects and the demonstrated applications are described by Waters and Wofsky (1978). Already, O_3 profile with 1 % precision ClO, H_2O_2, CO, H_2O, N_2O, NO with 10 % or better precision, for stratosphere has been obtained with aircraft-based limb sounding technique. Table 6 gives the application of microwave radiometric

Table 5. Some applications of airborne/spaceborne microwave radiometers in remote sensing (Ulaby *et al* 1981)

Hydrology:
Soil moisture distribution for river stage and flood forecasts.
Watershed surface drainage characteristics
Flood mapping
Identification of water surfaces
Snow cover extent, snow water equivalent and snow wetness.
Agriculture:
Soil moisture distribution for crop yield estimation and for irrigation scheduling.
Delineation of freeze than boundries.
Polar regions:
Monitoring and mapping sea-ice type
Mapping continental ice sheets.
Oceans:
Monitoring surface wind speeds
Monitoring surface temperature
Monitoring surface salinity
Monitoring surface oilspills
Severe storms:
Monitoring tropical cyclones (rain maps, temperature and humidity profiles, sea temperature and wind)
Severe local storms (temperature and humidity profiles, soil moisture and rain as feasible).
Meteorology and climatology (primary over oceans):
Temperature profile
Integrated water vapour
Water vapour profile
Liquid water (rain)
Ocean temperature and surface wind speed
Stratosphere, mesosphere and lower thermosphere:
Atmospheric temperature profile
Magnetic field profile
Abundance of atmospheric gases

techniques to upper atmospheric sensing and table 7 gives the measurement results till 1982 (Waters and Wofsky 1978). An example is shown in figure 13 for aircraft-based microwave measurements of H_2O in the upper atmosphere (Waters *et al* 1977). Other species have also been reported by Waters (1976).

8. Future prospects

The European, American, Russian, Japanese and Indian space agencies are including passive microwave radiometers within their earth remote sensing programme. The European space agency is planning to put imaging microwave radiometer (IMR) onboard ERS-1, for ocean monitoring. Japan is planning a marine observational satellite (MOS) and India, a scanning multichannel microwave radiometer as a follow-up of the satellite microwave radiometer onboard its previous two satellites *Bhaskara*-I and II. The application review panel (Staelin and Rosenkranz 1978) from NASA, and the study report on NOSS with LAMMR (large aperture multichannel microwave radiometer) are

Table 6. Applications of microwave radiometer techniques to upper atmospheric sensing (Waters 1978)

Stratospheric research and monitoring:
Measurement of temperature and minor constituents important to stratospheric chemistry.
Precision monitoring of ozone profiles (1% accuracy with better than 3 km vertical resolution should be achievable).
Mesospheric and lower thermospheric research:
Determine meteorology (temperature, winds) at mesopause region.
Why is mesopause coldest where maximum solar heating occurs?
Measure minor constituents important to mesospheric chemistry.
Measure O_2 in region where it is photodissociated by solar UV.
Although O_2 is the first major atmospheric gas to be dissociated by Solar UV and is thereby responsible for formation of ozone and heating of lower thermosphere, no techniques now exist or planned for measuring it, global measurements over daily and seasonal cycles should provide significant new information on solar terrestrial interactions.
Measure magnetic field disturbances in mesospheric and lower thermosphere (by Zeeman splitting of O_2 lines)
The charged solar particles are sensed by their disturbance of the terrestrial magnetic field. Simultaneous composition measurements will indicate their chemical interactions.

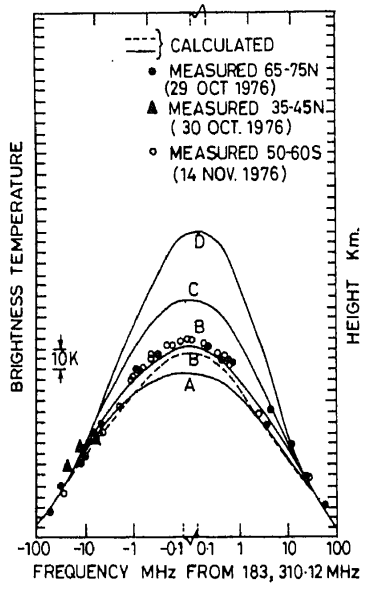

Figure 13. Aircraft-based microwave measurements of H_2O in the upper atmosphere (Waters *et al* 1977). Calculated and measured emission from the 183 GHz H_2O profiles, using US standard atmosphere. The zero level is arbitrary and the calculated and measured curves have been shifted slightly (~ 10 K) to coincide at 100 MHz from line centre. Measurements within 0·2 MHz of centre are not available in the two northern hemisphere bounds because of interference in those two channels.

Table 7. Microwave sensing of the upper atmosphere measurement results to date (Waters 1978).

Ground based:
First measurement of mesospheric carbon monoxide.
First continuous measurement of mesospheric ozone through a diurnal cycle.
Detection of mesospheric water vapour emission. Measurement of high-rotational emission lines of stratospheric O_2.
Aircraft based:
Measurement of stratospheric emission from 15 ozone microwave lines and recovery of ozone profiles.
First measurement of latitudinal variation in upper stratospheric and mesospheric water vapour.
Upper limit and tentative detection of stratospheric CIO radical.
Detection of emission from stratospheric nitrogen oxide (N_2O).
Demonstration of capability to measure variations in upper stratospheric temperature.
Satellite based:
Global measurements of lower stratospheric temperatures.

some of the examples of NASA'S interest in passive microwave radiometry. Besides, Topex (ocean topographic experiment) is already an ongoing activity of NASA and is being pursued at JPL. Some of these sensors are likely to be flown on space shuttles *e.g.* AMSU, MPS, MLS etc. India, having succeeded in launching microwave radiometers onboard its previous two satellites *Bhaskara*-I and II, (table 8) should now plan for more advanced microwave radiometer systems on its future mission, so that the momentum gained and the expertise acquired in analysing passive microwave radiometric data are not lost.

9. Conclusion

This article attempts to give a brief but a comprehensive overview of the state-of-the-art for remote sensing of the atmosphere and ocean. Emphasis has been on passive microwave radiometry with brief mention of active technique for some of the applications. References to the published work should be considered as representative rather than all inclusive; however, high resolution microwave sensors together with more traditional visible and IR sensors are likely to provide more insight into the oceanic and atmospheric processes and may lead to new advances and exciting discoveries. One can only hope that necessary resources would be available in future to exploit these modern tools for atmospheric and oceanographic research.

Acknowledgements

The authors thank Prof. E V Chitnis, Director, Prof. P D Bhavsar, Chairman, RSA and Shri O P N Calla, Chairman, Communications Area for their interest and encouragement. Thanks are due to Shri B S Gohil, Shri R M Gairola, Shri Rajkumar, Dr S M Bhandari, Dr Abhijit Sarkar and Dr P S Desai, who helped in various ways for the completion of this article. Shri Gopinathan provided excellent secretarial support which is gratefully acknowledged. Thanks are also due to Dr H S S Sinha for reading the manuscript and providing valuable suggestions.

Table 8. Characteristics of the SAMIR systems on board Bhaskara-I and II.

System parameter	Bhaskara-I radiometers			Bhaskara-II radiometers		
	R-1	R-2	R-3	R-1	R-2	R-3
Frequency (GHz)	19·1	19·6	22·235	31·4	19·35	22·235
RF Bandwidth (MHz)	250	250	250	250	250	250
Integration time (m sec)	350	350	470	300	300	300
RMS temperature sensitivity T(°K)	1	1	1	1	1	1
System noise figure (dB)	6·5	6·5	7·5	8·5	6·5	7·5
Spatial resolution (kM)	150	150	230	125	125	125
View angles with respect to Nadir (normal mode)	±2·8°, ±5·6° 180° (zenith)	±2·8°, ±11·2° 180° (zenith)		±2·8°, ±5·6°,	180° (zenith)	
View angles with respect to Nadir (alternate mode)	±2·8°, ±8·4°, ±14·0°, ±19·6°, ±25·2°, ±30·8°, ±36·4°					

References

Adler R F and Rodgers E B 1977 *Mon. Weath Review* Vol. 15 p. 956

Allison L J, Rodgers E B, Wilheit T T and Fett R W 1974 *Bull. Am. Meteor Soc.* **55** 1074

Alishouse J C 1982 *Tech. Report No.* 90 National Oceanic and Atmospheric Administration, Washington DC

Atlas D and Thiele O 1982 *Precipitation measurement from space*, Workshop Report, Goddard Space Flight Centre, Greenbelt, Maryland, USA

Basharinov A E, Gurvich A S and Yegorov 1969 *Dok. Acad. Nauk SSSR*, **188** 18

Bernstein R L (ed), 1982 *J. Geophys. Res.* (SEASAT *Special issue*) I. Geophysical Evaluation, Vol. 87

Blume H J C, Kendel B M and Fedors J C 1978 *Boundary-Layer Meteorol.* **13** 295

Campbell W J, Ramsier R O, Zwally H J and Gloerseu P 1980 *Boundary-Layer Meteorol.* **18** 99

Chahine M T 1977 *Inversion methods in atmospheric remote sounding*, (ed) A Deepak (New York: Academic Press), p 67

Desai P S 1982 MET-SN-14-82, Space Applications Centre, Ahmedabad

Flower D A 1978 *Microwave pressure sounder*, Publication 78-68, (Pasadena California USA: Jet Propulsion Laboratory)

Gately C, Pekham G E and Flower D A 1983 *Int. J. Remote Sensing* **4** 457

Gloersen P, Zwally H J, Chang A T C, Hall D K, Campbell W J and Ramsier R O 1978 *Boundary-Layer Meteorol.* **13** 339

Gloersen P and Barath F T 1977 *IEEE J. Oceanic Eng.* **OE-2** 172

Gohil B S, Hariharan T A, Pandey P C and Sharma A K 1982 *Int. J. Remote Sensing*, **3** 235

Grody N C 1976 *IEEE Trans. Antennas Prop.* **AP24** 153

Hariharan T A and Pandey P C 1983 *Proc. Indian Acad. Sci. (Engg. Sci.)* **6** 233

Haydu K J and Krishnamurthy T N 1983 *J. Appl. Meteor.* **20** 1177

Hofev R, Njoku E G and Waters J W 1981 *Science* **212** 1385

Hofev R and Njoku E G 1981 *IEEE Trans. Geosci. Remote Sensing* **GE-19** 178

Hollinger J P 1971 *IEEE Trans. Geosci. Electr.* **GE-9** 165

Hollinger J P and Mannella 1973 *Science* **181** 54

Hollinger J P 1974 Report 2953, Naval Research Laboratory, Washington, USA

ISRO Report 1981 *Analysis of data collected by microwave radiometer onboard Bhaskara*, Technical Report TR-16-81, Indian Space Research Organization, Bangalore, India

Kunzi K F, Fisher A D, Staelin D H and Waters J W 1976 *J. Geophys. Res.* **81** 4965

Ledsham W H and Staelin D H 1978 *J. Appl. Meteor.* **17** 1023

Lipes R G 1980 Publication 80-62, JPL Pasadena, Calif, USA

Moore R K and Young J D 1977 *IEEE J. Oceanic Eng.* **OE-2** 309

Nelepo B A, Armand N A, Khmyrov B E, Terekhin Yu. V, Kutüza B G, Bushnev E I 1982 *Issled. Zenlic Kosmasa* (in Russian), No. 3 p 5

Newton R W 1976 Microwave remote sensing and its application to soil moisture detection, Technical Report RSC-83, Remote Sensing Centre, Texas A and M University college station, Texas.

Njoku E G and Swanson L 1983 *Mon. Weath. Rev.* (submitted)

Njoku E G 1982 *Proc. IEEE*, **70** 728

Njoku E G, Christensen E J, Cofield R E 1980 *IEEE J. Oceanic Eng.* **OE-5** 125

Njoku E G 1980 *Boundary Layer Meteor.* **18** 79

Njoku E G, Stacey J M and Farath F T 1980 *IEEE J. Oceanic Eng.*, **OE-5** 200

Pathak P N, Desai P S and Hariharan T A 1983 *Indian J. Radio Phys.* Vol. 12 p. 141

Pandey P C and Kakar R K 1983 *IEEE Geosci. Remote Sensing* **GE-2** 208

Pandey P C and Kakar R K 1982 *IEEE J. Oceanic Eng.* **OE-7** 135

Pandey P C 1983 Publication No. 83-5, Jet Propulsion Laboratory, Pasadena, Calif., USA

Pandey P C 1982 Publication No. 82-95, Jet Propulsion Laboratory, Pasadena, Calif., USA

Pandey P C and Kniffen S 1982 Publication No. 82-89, Jet Propulsion Laboratory, Pasadena, Calif., USA

Pandey P C, Gohil B S, Sharma A K 1981 *Mausam* **32** 17

Pandey P C, Gohil B S and Hariharan T A 1983 A two-frequency differential technique for retrieving precipitable water from SAMIR-II onboard Bhaskara-II, paper presented in International Geoscience and Remote Sensing Symposium (IGARSS 1983) held at San Francisco

Pandey P C, Njoku E G and Waters J W 1983 *J. Clim. Appl. Meteorol.* Vol. 22 p. 1894

Pekham G E, Flower D A 1983 *Int. J. Remote Sensing* **4** 457

Prabhakar C, Chang H D and Chang A T C 1982 *J. Appl. Meteor.* **21** 59

Rosenkranz P W 1978 *Radio Sci.* **13** 1003
Rosenkranz P W and Staelin D H 1982 *J. Appl. Meteor.* **21** 1364
Satellite derived Sea Surface Temperature, Workshop-I, No. 83-84, Jet Propulsion Laboratory, Pasadena, California, USA
Savage R C 1976 *The transfer of thermal microwaves through hydrometers*, Ph.D. Thesis (Meteorology), University of Wisconsin, Madison, pp 147
Schmugge T J, Gloersen P, Wilheit T and Geiger F 1974 *J. Geophys. Res.* **79** 317
Schmugge T J 1978 *J. Appl. Meteor.* **17** 1549
Shaerer G and Wilheit T T 1979 *Radio Sci.* **14** 371
Saxton J A and Lane J A 1952 *Wireless Eng.* **29** 269
Staelin D H 1981 *IEEE Trans. Antennas Propagat*, **AP-29** 693
Staelin D H, Cossel A L, Kunzi K F, Pettyjohn R L, Poon R K L and Rosenkranz P W 1975 *J. Atmos. Sci.* **32** 1970
Staelin D H, Kunzi K F, Petty John R L, Poon R K L and Wilcox R W 1976 *J. Appl. Meteor.* **15** 1204
Swift C T 1980 *Boundary-Layer Meteor.* **18** 25–54
Staelin D H and Rosenkranz P W 1978 Application panel, high resolution passive microwave satellites, Final Report, Research Laboratory of Electronics, Massachussetts Institute of Technology, Cambridge, Mass, USA
Thomann G C 1976 *IEEE Trans. Geosci. Electr.* **GE-14** 198
Tomiyasu K 1974 *Proc. IEEE* **62** No. 1
Ulaby F T, Moore R K and Fung A K 1981 *Microwave remote sensing fundamentals and radiometry*, (Reading, Mass: Addison-Wesley), Vol 1
Ulaby F T 1976 *IEEE Trans. Antennas Propag.* **AP-24** 112
Waters J W 1976 Absorption and emission by atmospheric gases in *Methods of experimental physics*, (ed) M L Meeks (New York: Academic Press) Vol 12 pp 172
Waters J W, Kunzi K F, Petty John R L, Poon R K L and Staelin D H 1975 *J. Atmos. Sci.* **32** 1953
Waters J W, Wilson W J and Shimabukuro 1976 *Science* **191** pp 1174
Waters J W and Wofsy S C 1978 In *High resolution passive microwave satellites*, (eds) D H Staelin and P W Rosenkranz (Cambridge, MA: MIT Research Lab of Electronics)
Weinman J A and Davies R 1978 *J. Geophys. Res.* **83** 3100
Wentz F J 1983 *J. Geophys. Res.* **88** 1892
Wilheit T T and Chang A T C 1980 *Radio Sci.* **15** 525
Wilheit T T 1979 *IEEE Trans. Geosci. and remote sensing* **GE-17** 244
Wilheit T T, Chang A T C, King J L, Rodgers E B, Nieman R A, Krupp B M, Milman A S, Stratigos J S and Siddalingaiah J H 1982 *J. App. Meteor.* **21** 1137
Wilheit T T, Nordberg W, Blinn J, Campbell W J and Edgeston A 1972 *Remote Sensing Environ.* **2** 129
Wilheit T T, Chang A T C, Rao M S V, Rodgers E B and Theon J S 1977 *J. Appl. Met.* **16** pp 551